



Charge transfer and formation of Ce^{3+} upon adsorption of metal atom M ($M = \text{Cu}, \text{Ag}, \text{Au}$) on CeO_2 (100) surface

Li-Jiang Chen^a, Yuanhao Tang^a, Lixia Cui^a, Chuying Ouyang^c, Siqi Shi^{a,b,*}

^aSchool of Sciences, Zhejiang Sci-Tech University, Xiasha College Park, Hangzhou 310018, China

^bSchool of Materials Science and Engineering, Shanghai University, Shanghai 200444, China

^cDepartment of Physics, Jiangxi Normal University, Nanchang 330022, China

HIGHLIGHTS

- Adsorption of M ($M = \text{Cu}, \text{Ag}, \text{Au}$) on $\text{CeO}_2(100)$ causes in charge transfer from M to Ce .
- For the same adsorption site, there exist multiple adsorption configurations.
- Our theoretical results are compared wherever possible with experiment.

ARTICLE INFO

Article history:

Received 7 December 2012

Received in revised form

16 January 2013

Accepted 18 January 2013

Available online 28 January 2013

Keywords:

Ceria (100) surface

Charge redistribution

Adsorption energy

First-principles calculations

ABSTRACT

Adsorption behavior of metal atom M ($M = \text{Cu}, \text{Ag}, \text{Au}$) on $\text{CeO}_2(100)$, a technologically important catalytic support surface, is studied by using first-principles density-functional theory calculations with the on-site Coulomb interaction taken into account (DFT + U). Prior to geometry optimization, small distortions in selected $\text{Ce}-\text{O}$ distances are imposed to explore the energetics associated with reduction of Ce^{4+} to Ce^{3+} due to charge transfer to Ce during M adsorption. Results indicate that the adsorption is accompanied by an electron charge transfer between neutral metal atom and neighboring Ce^{4+} cation. For the same adsorption site, there exist multiple adsorption configurations with the excess electron localized at various nearest neighboring Ce ion relative to the M . The order on adsorption energies of M on $\text{CeO}_2(100)$ surface follows: $\text{Cu} > \text{Au} > \text{Ag}$. The atomic and electronic structures of M on $\text{CeO}_2(100)$ are compared with those of M on $\text{CeO}_2(111)$ and $\text{CeO}_2(110)$.

© 2013 Elsevier B.V. All rights reserved.

1. Introduction

Materials based on CeO_2 have attracted much attention because of their uses in a variety of processes such as automotive exhaust catalysis, water-gas shift (WGS) reactions, fuel cells and production or purification of hydrogen [1,2]. These applications of CeO_2 are largely attributed to its remarkable oxygen-storage capability and the strong interaction between loaded metal atom and CeO_2 support [3]. This has been confirmed by examining the oxidation of CO [4], reduction of NO_x [5] and destruction of SO_2 [6] on metal nanoparticles dispersed on CeO_2 . Some investigations [7–13] have shown that the dispersion of M ($M = \text{Cu}, \text{Au}, \text{Pt}, \text{Rh}$) in a CeO_2 matrix can produce materials with novel structural and/or electronic properties, especially the formation of the ionic $M-\text{O}$ bonds,

playing an important role in the conversion of CO (NO or SO_2) in M/CeO_2 catalysts. In other words, the kinetic behaviors of the CeO_2 supported catalysts depend strongly on the morphology and chemical state of the active metal species. For example, Kydd et al. [7] and Avgouropoulos et al. [13] have observed the conversion of CO in the Cu/CeO_2 system with $\text{Cu}-\text{O}$ or $\text{Cu}-\text{O}-\text{Ce}$ bonds by Flame Spray Pyrolysis (FSP), Brunauer–Emmett–Teller (BET) adsorption isotherms, X-ray diffraction (XRD), High Resolution Transmission Electron Microscopy (HRTEM), Temperature Programmed Reduction (TPR) and Temperature Programmed Desorption (TPD).

Performance of CeO_2 supported catalysts is also relevant to the electronic structures of the adsorbed metal atom. It is generally recognized that the adsorbed metal atom is oxidized and thus brings in transformation of $\text{Ce}^{4+} \rightarrow \text{Ce}^{3+}$. The adsorbed metal ions are active in the oxidation catalytic reaction. Some theoretical investigations have revealed that the metal atoms could form relatively strong bonds with oxygen atoms by transferring their outer electron to the substrate and thus CeO_2 surface is reduced. For example, Branda et al. [14] and Tang et al. [15] have investigated the adsorption behavior of

* Corresponding author. School of Sciences, Zhejiang Sci-Tech University, Xiasha College Park, Hangzhou 310018, China. Tel./fax: +86 571 86843655.

E-mail address: siqishihz@gmail.com (S. Shi).

Cu, Ag and Au on $\text{CeO}_2(111)$ surface and found M^+ ($M = \text{Cu}, \text{Ag}, \text{Au}$). Hernández et al. [16] suggested that the high activity of $\text{Au}/\text{CeO}_2(111)$ system should be due to Au ions resulting from charge transfer from Au to Ce atom. Therefore, it is of great importance to clarify the effect of the adsorption of metal atom on its electronic states or the charge redistribution at the M/CeO_2 interfaces.

Studies on atomic and electronic structure of metal atom M ($M = \text{Cu}, \text{Ag}, \text{Au}$) on the $\text{CeO}_2(111)$ and (110) surfaces can be found in Refs. [14–20]. In our preceding papers [15,17], we have made detailed analyses on the adsorption behaviors of metal M ($M = \text{Cu}, \text{Ag}, \text{Au}$) atom on $\text{CeO}_2(111)$ and (110) surfaces by using first-principles calculations based on density functional theory (DFT). Charge redistributions with electron localized on various Ce cations neighboring to adsorbed atom M ($M = \text{Cu}, \text{Ag}, \text{Au}$) are observed and can be attributed to local structural distortion effects. We demonstrate that the electron localized on the Ce ion away from the metal M ($M = \text{Cu}, \text{Ag}, \text{Au}$) atom and the adatom is oxidized to be M^+ on $\text{CeO}_2(111)$ and $\text{CeO}_2(110)$ surfaces, and Cu adatom on $\text{CeO}_2(110)$ surface can also be oxidized to Cu^{2+} . More importantly, previous controversies about the valence state of the adsorbed Au atom on $\text{CeO}_2(111)$ surface have been successfully clarified via analysis of the local structural distortions [15]. Nevertheless, a careful examination of the literature revealed no other attempts to use first-principles calculation to study the adsorption behavior of M adsorption on $\text{CeO}_2(100)$. Following the classification by Sayle et al. [21], $\text{CeO}_2(100)$ surface can be described as the kind of one, on which exists a net dipole normal to the surface. Such a surface would be described as a polar one and predicted to have a high surface energy or catalytic activity [22–31]. Besides, several studies [24,31,32] have indicated that the (100) surface undergoes a drastic structure rearrangement by usage of scanning tunneling microscope (STM), low energy electron diffraction (LEED) and the molecular dynamics simulation. Accordingly, compared with the non-polar (111) and (110) surfaces, the polar (100) surface seems more reactive and consequently more important to comprehensively understand the catalytic behaviors of M/CeO_2 ($M = \text{Cu}, \text{Ag}, \text{Au}$) systems. For

example, experimental works of Zhou et al. [33] and Aneghi et al. [34] have provided an evidence of the surface sensitivity of the $\text{CO}-\text{CeO}_2$ interaction by studying the catalytic activity of CeO_2 nanorods and nanoparticles and polycrystalline CeO_2 ; it was demonstrated that CeO_2 nanorods, with well-defined reactive planes (001) and (110) , are more active than “classical” ceria nanoparticles with the (111) planes. Trtik et al. [35] prepared $\text{CeO}_2(001)$ epitaxial thin films deposited on $\text{Si}(001)$ with yttria-stabilized zirconia buffers at room temperature by pulsed-laser deposition. Therefore, it is worthwhile to investigate the relative stabilities and electronic redistribution of the adsorption of Cu, Ag or Au on the (100) surface of ceria and to ascertain whether the polarity and instability of the $\text{CeO}_2(100)$ surface would in turn affect the adsorption structures or electronic properties of metal atom on CeO_2 surfaces.

In this paper, we examine the effect of the adsorption of M ($M = \text{Cu}, \text{Ag}, \text{Au}$) atom on the Ce-4f electron localization on $\text{CeO}_2(100)$ surface and the associated structural stability by using the first-principles calculations based on the density functional theory (DFT). We find the most energetically favorable structure is M adsorption on O-bridge (O_u-O_u) site. Charge redistributions, with electrons localized on 1NN, 2NN and 3NN (The 1NN, 2NN and 3NN notations represent the Ce ions which are the first, second and third nearest neighbors to the adatoms, respectively.) Ce ions to M are observed with Ce^{4+} reduced to Ce^{3+} in most cases. In addition, a detailed comparison of the atomic and electronic structure of M on $\text{CeO}_2(111)$ and (110) surfaces is made for the selected adsorption sites. An important difference from our previous studies on M ($M = \text{Cu}, \text{Ag}, \text{Au}$) on $\text{CeO}_2(111)$ and (110) surfaces [15,17] is the observation that the M adsorption configuration with the excess electron located at the first nearest neighboring Ce^{4+} ion is more energetically favorable. The present methodology and results provide a useful basis of comparison for experimental studies focused on catalyst designs.

The computational details are outlined in Section 2. And Section 3 details the adsorption models, energetics, and discussions of the major theoretical predictions. The most significant conclusions from this study are listed in Section 4.

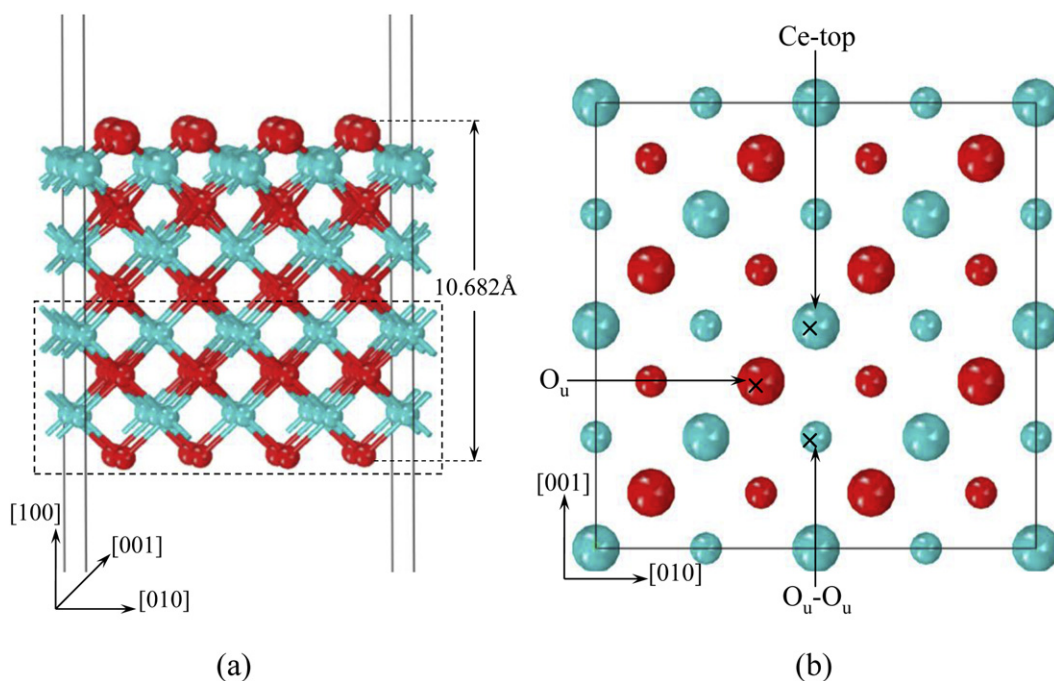


Fig. 1. $\text{CeO}_2(100)$ $p(2 \times 2)$ surface and M ($M = \text{Cu}, \text{Ag}, \text{Au}$) adsorption sites (labeled as “x”). (a) Oblique view along $[001]$; (b) View of surface along $[100]$. Red and blue spheres represent O and Ce, respectively. Large spheres denote the first layer ions. (For interpretation of the references to color in this figure legend, the reader is referred to the web version of this article.)

2. Computational details and supercell construction

The fully spin-polarized calculations are performed by using the frozen-core all-electron projected augmented wave (PAW) method [36], as implemented in the *ab initio* total energy and molecular dynamic program VASP (the Vienna *ab initio* simulation package) [37]. The Perdew–Burke–Ernzerhof (PBE) functional [38] is used for the exchange correlation. To account for strong on-site Coulomb repulsion among the Ce 4*f* electrons, a Hubbard parameter *U* is added to the PBE functional with the rotationally invariant approach formulated by Dudarev et al. [39], in which only the difference ($U_{\text{eff}} = U - J$) between the Coulomb *U* and exchange *J* parameters must be specified. As suggested by Fabris et al. [40] for

CeO₂ using the linear-response approach of Cococcioni and de Gironcoli [41], the U_{eff} value of 4.5 eV is used. The choice of this methodology (including PBE functional, rotationally invariant approach and U_{eff} value) is supported by previous studies on CeO₂ systems that have shown a very good agreement with available results for bulk CeO₂ and CeO₂(111) and (110) surfaces [15,17,42–45]. The present PBE + *U* calculations give an equilibrium lattice parameter of 5.49 Å [46], which is close to the experimental value of 5.41 Å [47,48].

Valence electron configurations for the elemental constituents are as follows: Ce-5*s*²5*p*⁶6*s*²5*d*¹4*f*¹, O-2*s*²2*p*⁴, Cu-3*d*¹⁰4*s*¹, Ag-4*d*¹⁰5*s*¹ and Au-5*d*¹⁰6*s*¹. The Monkhorst–Pack scheme [49] based on the 2 × 2 × 1 *k*-point grid and the Gaussian smearing of 0.20 eV

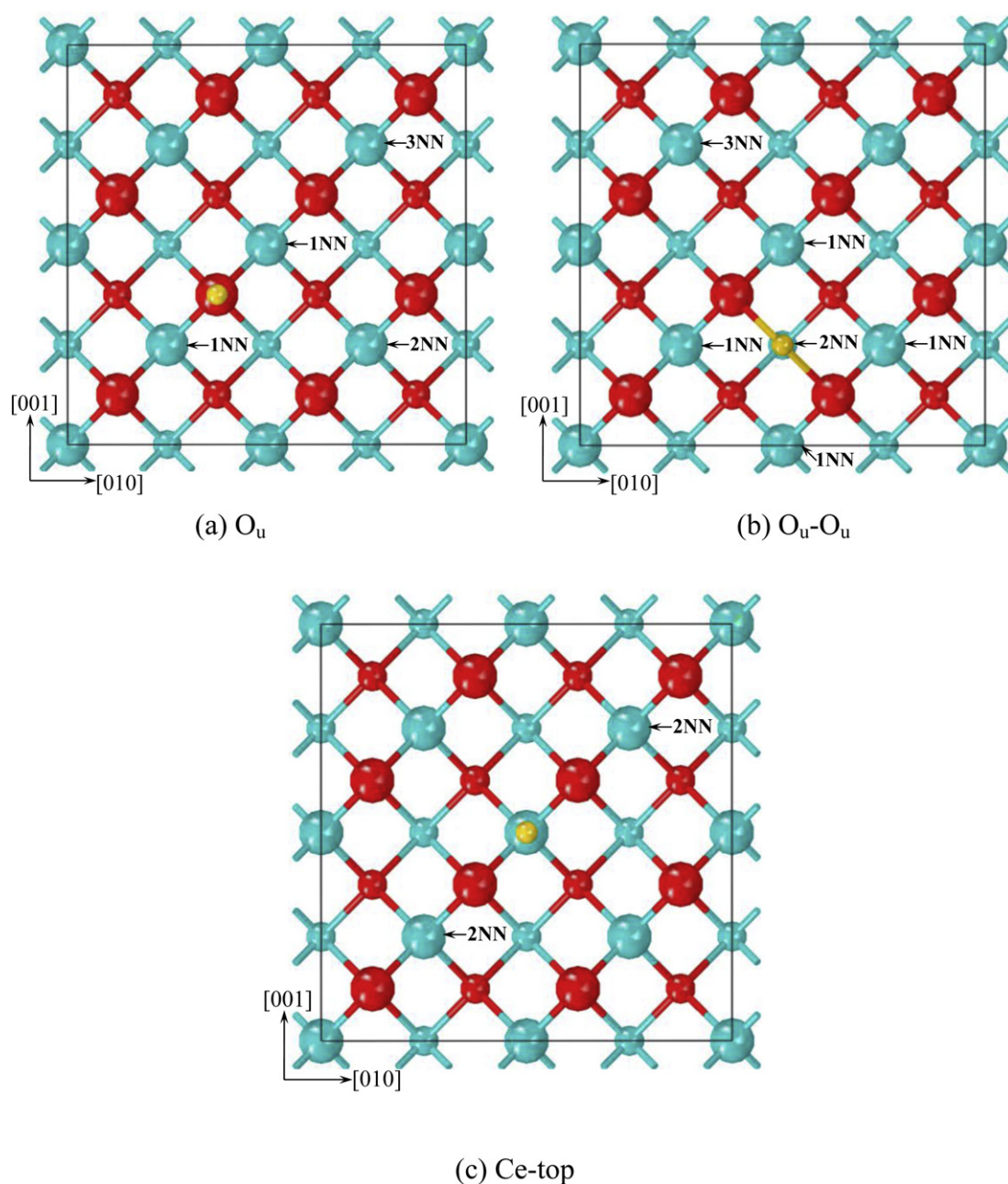


Fig. 2. Structural models of *M* (*M* = Cu, Ag, Au) atoms adsorbed on CeO₂(100). (a) O_u (O-top), (b) O_u-O_u (O-bridge), (c) Ce-top. Red, blue and yellow spheres denote O, Ce and *M* atoms, respectively. The 1NN to 3NN notations indicate the Ce ions which are first, second and third nearest neighbors, respectively, to the adsorbed *M* atom. (For interpretation of the references to color in this figure legend, the reader is referred to the web version of this article.)

Table 1

Adsorption energies, bond lengths and magnetic spin moments of metal atoms for the adsorption configurations of Cu atom on CeO₂(100). For a given adsorption site, configuration numbers (e.g. conf. 2, 1NN) are associated with the distortion applied to Ce–O distances listed as $d_{\text{Ce-O}}$, which are the bond lengths between the Ce³⁺ and the nearest neighboring O ions. The undistorted $d_{\text{Ce-O}}$ is 2.38 Å. E_{ads} is the computed adsorption energy, $d_{\text{Cu-O}}$ is the distance between the adsorbed Cu and the nearest neighboring O ions (an O ion for the O_u site and two O ions for the O_u–O_u and Ce-top sites), and $d_{\text{Cu-Ce}}$ are distances from the adsorbed Cu to 1NN, 2NN, and 3NN Ce ions (1NN, the first nearest neighbor, 2NN, the second nearest neighbor and 3NN, the third nearest neighbor Ce ion from the Cu adatom), respectively, following geometry optimization. Note that integers in $d_{\text{Cu-O}}$ (Å) and $d_{\text{Cu-Ce}}$ (Å) denote the number of O and Ce ions, respectively, within the distances relative to the adsorbed Cu ion. Magnetic spin moments of reduced Ce (in bold) and oxidized Cu ions are, respectively, μ_{Ce} and μ_{Cu} .

Site	E_{ads} (eV)	$d_{\text{Cu-O}}$ (Å)	$d_{\text{Cu-Ce}}$ (Å)	$\mu_{\text{Ce}}(\mu_{\text{B}})$	$d_{\text{Ce-O}}$ (Å)	$\mu_{\text{Cu}}(\mu_{\text{B}})$
O _u (conf. 1)	2.093	1 × 1.772	1 × 3.667	0.526	1 × 2.429	0.000
			1 × 3.667	0.527	2 × 2.272	
			4 × 5.298	0.000	1 × 2.566	
			2 × 6.088	0.000	1 × 2.236	
O _u (conf. 2, 1NN)	2.376	1 × 1.773	2 × 6.603	0.000	1 × 2.422	0.000
			1 × 3.584	0.000	1 × 2.478	
			1 × 3.783	0.958	1 × 2.326	
			1 × 5.216	0.000	1 × 2.321	
			1 × 5.249	0.000	1 × 2.662	
			1 × 5.385	0.000	1 × 2.358	
			1 × 5.421	0.000	1 × 2.529	
			1 × 6.111	0.000		
			1 × 6.125	0.000		
			1 × 6.363	0.000		
			1 × 6.855	0.000		
			1 × 3.630	0.000	1 × 2.589	
O _u (conf. 3, 2NN)	2.296	1 × 1.768	1 × 3.656	0.000	1 × 2.332	0.000
			1 × 5.204	0.000	1 × 2.345	
			1 × 5.215	0.000	1 × 2.592	
			1 × 5.245	0.000	1 × 2.423	
			1 × 5.176	0.957	1 × 2.424	
			1 × 6.009	0.000		
			1 × 6.000	0.000		
			1 × 6.560	0.000		
			1 × 6.537	0.000		
			1 × 3.611	0.000	1 × 2.604	
O _u (conf. 4, 3NN)	2.316	1 × 1.772	1 × 3.663	0.000	1 × 2.332	0.000
			2 × 5.253	0.000	1 × 2.337	
			1 × 5.282	0.000	1 × 2.550	
			1 × 5.285	0.000	1 × 2.442	
			1 × 6.063	0.000	1 × 2.396	
			1 × 6.064	0.000		
			1 × 6.522	0.963		
			1 × 6.549	0.000		
			2 × 3.182	2 × 0.288	1 × 2.452	
			2 × 3.182	2 × 0.287	1 × 2.251	
O _u –O _u (conf. 1)	3.702	2 × 1.810	1 × 4.249	0.000	1 × 2.262	0.000
			2 × 5.744	0.000	1 × 2.539	
			2 × 5.786	0.000	1 × 2.197	
			4 × 6.312	0.000	1 × 2.378	
			1 × 3.149	0.000	1 × 2.491	
			1 × 3.158	0.000	1 × 2.319	
			1 × 3.225	0.000	1 × 2.347	
			1 × 3.254	0.958	1 × 2.674	
			1 × 4.259	0.000	1 × 2.349	
			1 × 5.748	0.000	1 × 2.572	
O _u –O _u (conf. 2, 1NN)	4.079	1 × 1.809 1 × 1.813	2 × 5.762	0.000		0.000
			1 × 5.843	0.000		
			1 × 6.242	0.000		
			1 × 6.249	0.000		
			1 × 6.286	0.000		
			1 × 6.311	0.000		
			1 × 3.193	0.000	1 × 2.484	
			1 × 3.197	0.000	1 × 2.421	
			1 × 3.199	0.000	1 × 2.419	
			1 × 3.207	0.000	1 × 2.486	
			1 × 4.264	0.859	1 × 2.403	
			1 × 5.776	0.000	1 × 2.576	
			1 × 5.786	0.000	1 × 2.586	
			1 × 5.811	0.000	1 × 2.403	
			1 × 5.812	0.000		
			1 × 6.332	0.000		
O _u –O _u (conf. 3, 2NN)	3.916	1 × 1.809 1 × 1.810	1 × 6.316	0.000		0.000
			1 × 6.328	0.000		
			1 × 6.319	0.000		
			1 × 3.178	0.000	1 × 2.573	
			1 × 3.184	0.000	1 × 2.332	
			1 × 3.186	0.000	1 × 2.333	
O _u –O _u (conf. 4, 3NN)	3.920	1 × 1.815 1 × 1.813				0.000

Table 1 (continued)

Site	$E_{\text{ads}}(\text{eV})$	$d_{\text{Cu-O}}(\text{\AA})$	$d_{\text{Cu-Ce}}(\text{\AA})$	$\mu_{\text{Ce}}(\mu_{\text{B}})$	$d_{\text{Ce-O}}(\text{\AA})$	$\mu_{\text{Cu}}(\mu_{\text{B}})$
Ce-top (conf. 1)	2.221	1×1.948 1×1.948	1×3.207	0.000	1×2.643	0.000
			1×4.261	0.000	1×2.378	
			1×5.743	0.000	1×2.392	
			1×5.783	0.000		
			1×5.790	0.000		
			1×5.800	0.000		
			1×6.244	0.909		
			1×6.326	0.000		
			1×6.266	0.000		
			1×6.347	0.000		
			1×2.444	0.000	1×2.530	
			1×4.510	0.000	1×2.237	
			1×4.599	0.000	1×2.243	
			1×4.602	0.600	1×2.469	
Ce-top (conf. 2, 2NN)	2.638	1×1.897 1×1.907	1×4.635	0.600	1×2.220	0.000
					1×2.192	
			1×2.710	0.000	1×2.633	
			1×4.078	0.000	1×2.304	
			1×4.632	0.000	1×2.311	
			1×4.675	0.000	1×2.378	
			1×5.370	0.969	1×2.293	
					1×3.463	

Distances between Cu and reduced Ce are labelled in bold.

are employed for the Brillouin-Zone integrals. The cutoff energy for the plane-wave is 400 eV. This set of parameters assures a total energy convergence of 10^{-7} eV unit cell $^{-1}$. The structure optimizations are performed until all the Hellmann–Feynman forces are converged to be less than 0.01 eV \AA^{-1} . For a more accurate calculation of the electronic density of states (DOS), we apply $4 \times 4 \times 1$ k -point grid and the modified tetrahedron method [50].

The (100) surface is modeled as an oxygen-terminated $p(2 \times 2)$ (p = primitive) slab (red enlarged spheres denote surface O ions in Fig. 1(a)) with half of the surface oxygen atoms moved from one side of the slab to the other in a checkerboard style to fulfill the CeO_2 formula and to avoid a dipole moment normal to the surface [32]. Fig. 1(a) shows the slab has a 26.98 \AA thickness and contains 32 CeO_2 formula units (nine atomic layers) and a vacuum layer of 16 \AA . The x [010] and y [001] dimensions of the slab are both fixed at the 10.98 \AA as shown in Fig. 1(b), which is based on the optimized 5.49 \AA CeO_2 lattice parameter. Although the relaxation in the $\text{CeO}_2(100)$ surface is complex (because of the removal of half a monolayer of outer oxygen atoms) as compared with the (111) and (110) surfaces, surface energy convergence tests [23] show that relaxation in the $\text{CeO}_2(100)$ surface occurs within the initial five layers and the atomic structures at the center of the slabs are bulk-like. Our calculated results show that the interlayer distance in the Ce sublattice increases slightly (expanded ca. 0.04 \AA near the surface). The original coplanar O atoms in the third and fifth atomic layers are split into two sets with the separation of 0.46 and 0.17 \AA , respectively. The bottom four layers are fixed at their bulk positions (see region enclosed by dashed line in Fig. 1(a)) and remaining layers are allowed to relax. (For interpretation of the references to color in this paragraph, the reader is referred to the web version of this article.)

Fig. 1(b) shows three adsorption positions of M ($M = \text{Cu}, \text{Ag}, \text{Au}$) atoms on the $\text{CeO}_2(100)$ surface. Here, the following definitions apply: O_u (a surface O-top site); $\text{O}_u\text{--O}_u$ (a surface O-bridge site), and Ce-top (a surface Ce-top site). Each occurrence of \times in Fig. 1(b) denotes an M adsorption site on $\text{CeO}_2(100)$. Fig. 2 shows the position of an adsorbed M (yellow) at O_u , directly above a surface O ion (Fig. 2(a)), $\text{O}_u\text{--O}_u$, an oxygen ion bridge site (Fig. 2(b)), and Ce-top, a Ce ion top site (Fig. 2(c)) on $\text{CeO}_2(100)$ surface. This is different from previous studies of $M/\text{CeO}_2(111)$ and $M/\text{CeO}_2(110)$, where four (O_d , O_u , $\text{O}_u\text{--O}_u$, Ce–Ce) and three (O_u , $\text{O}_u\text{--O}_u$, Ce–Ce) adsorption

sites must be considered. (For interpretation of the references to color in this paragraph, the reader is referred to the web version of this article.)

Prior to geometry optimization, small structural distortions were introduced into the as-built models to achieve various localized solutions. This required slight adjustment of distances between a Ce^{4+} ion and its nearest-neighboring O ions to be consistent with those of a Ce^{3+} ion. The positions of M on the surface and the associated bond length adjustments resulted in a range of model configurations which we now explore. Experimentally, these slight distortions can be realized by introducing impurities or manipulating the crystal morphology during catalytic material preparation [51,52]. The adsorption energy, E_{ads} , of M atom on $\text{CeO}_2(100)$ is calculated via:

$$E_{\text{ads}} = E_{\text{CeO}_2} + E_M - E_{M/\text{CeO}_2} \quad (1)$$

where E_{CeO_2} , E_M and E_{M/CeO_2} correspond to the calculated total energies of the clean $\text{CeO}_2(100)p(2 \times 2)$, isolated M atom and combined $M/\text{CeO}_2(100)p(2 \times 2)$ system, respectively.

3. Results and discussion

Identified by computing E_{ads} are the Ce^{3+} location, the $M\text{--O}$, $M\text{--Ce}$ and Ce--O bond lengths, magnetic spin moments of M and Ce, and various configurations for 4f electrons localized at neighboring Ce ions to the M ($M = \text{Cu}, \text{Ag}, \text{Au}$). These quantities are listed in Tables 1–3 for Cu, Ag and Au, respectively. Results without small structural distortions at three sites are also listed, although the following discussion only refers to the distorted cases unless otherwise explicitly stated. We consider the $\text{O}_u\text{--O}_u$ adsorption site (shown in Fig. 2(b)) as an example. There are three different distances of Ce^{3+} ions around the adsorbed M ion. These are denoted as 1NN, 2NN and 3NN, respectively, as mentioned above. The computed spin moments of Ce and Cu in Table 1 show that the s electron from the Cu atom can localize on neighboring Ce ions since $\text{Cu-}3d^{10}$ has no moment associated with it. Note that for the $\text{O}_u\text{--O}_u$ site, the 2NN Ce ion is located in the subsurface (i.e., the fourth atomic layer in Fig. 1(a)) whereas the 1NN and 3NN Ce ions are at the surface (i.e., the second atomic layer in Fig. 1(a)). This is opposite to the case of the $\text{O}_u\text{--O}_u$ site for $M/\text{CeO}_2(110)$, and is

Table 2

Adsorption energies, bond lengths and magnetic spin moments of metal atoms for the adsorption configurations of Ag atom on CeO₂(100). For a given adsorption site, configuration numbers (e.g. conf. 2, 1NN) are associated with the distortion applied to Ce–O distances listed as $d_{\text{Ce-O}}$, which are the bond lengths between the Ce³⁺ and the nearest neighboring O ions. The undistorted $d_{\text{Ce-O}}$ is 2.38 Å. E_{ads} is the computed adsorption energy, $d_{\text{Ag-O}}$ is the distance between the adsorbed Ag and the nearest neighboring O ions (an O ion for the O_u site and two O ions for the O_u–O_u and Ce-top sites), and $d_{\text{Ag-Ce}}$ are distances from the adsorbed Ag to 1NN, 2NN, and 3NN Ce ions (1NN, the first nearest neighbor, 2NN, the second nearest neighbor and 3NN, the third nearest neighbor Ce ion from the Ag adatom), respectively, following geometry optimization. Note that integers in $d_{\text{Ag-O}}$ (Å) and $d_{\text{Ag-Ce}}$ (Å) denote the number of O and Ce ions, respectively, within the distances relative to the adsorbed Ag ion. Magnetic spin moments of reduced Ce (in bold) and oxidized Ag ions are, respectively, μ_{Ce} and μ_{Ag} .

Site	E_{ads} (eV)	$d_{\text{Ag-O}}$ (Å)	$d_{\text{Ag-Ce}}$ (Å)	$\mu_{\text{Ce}}(\mu_{\text{B}})$	$d_{\text{Ce-O}}$ (Å)	$\mu_{\text{Ag}}(\mu_{\text{B}})$
O _u (conf. 1)	1.307	1×2.059	$1 \times \mathbf{3.858}$	0.496	1×2.448	0.000
			$1 \times \mathbf{3.858}$	0.495	2×2.272	
			4×5.440	0.000	1×2.557	
			2×6.324	0.000	1×2.247	
			2×6.711	0.000	1×2.379	
O _u (conf. 2, 1NN)	1.437	1×2.062	1×3.703	0.000	1×2.486	0.000
			$1 \times \mathbf{4.057}$	0.901	2×2.307	
			1×5.315	0.000	1×2.642	
			1×5.310	0.000	1×2.356	
			1×5.595	0.000	1×2.506	
			1×5.589	0.000		
			1×6.341	0.000		
			1×6.338	0.000		
			1×6.320	0.000		
			1×7.108	0.000		
			1×3.879	0.000	1×2.584	
			1×3.862	0.000	1×2.323	
O _u (conf. 3, 2NN)	1.369	1×2.067	$1 \times \mathbf{5.360}$	0.887	1×2.326	0.000
			1×5.371	0.000	1×2.589	
			1×5.406	0.000	1×2.402	
			1×5.402	0.000	1×2.401	
			1×6.299	0.000		
			1×6.291	0.000		
			1×6.708	0.000		
			1×6.699	0.000		
			1×3.842	0.000	1×2.592	
			1×3.880	0.000	1×2.333	
O _u (conf. 4, 3NN)	1.561	1×2.066	1×5.447	0.000	1×2.328	0.000
			1×5.446	0.000	1×2.567	
			1×5.423	0.000	1×2.446	
			1×5.420	0.000	1×2.411	
			$1 \times \mathbf{6.641}$	0.962		
			2×6.336	0.000		
			1×6.666	0.000		
			$2 \times \mathbf{3.325}$	2 × 0.263	1×2.450	
			$2 \times \mathbf{3.325}$	2 × 0.264	1×2.245	
O _u –O _u (conf. 1)	2.045	2×2.077	1×4.501	0.000	1×2.264	0.000
			2×5.950	0.000	1×2.534	
			2×5.975	0.000	1×2.204	
			4×6.383	0.000	1×2.358	
			1×3.301	0.000	1×2.499	
			1×3.310	0.000	1×2.323	
			1×3.378	0.000	1×2.339	
			$1 \times \mathbf{3.378}$	0.960	1×2.638	
			1×4.532	0.000	1×2.362	
			1×5.952	0.000	1×2.557	
O _u –O _u (conf. 2, 1NN)	2.437	2×2.070	1×5.970	0.000		0.000
			1×5.984	0.000		
			1×6.041	0.000		
			1×6.325	0.000		
			1×6.404	0.000		
			1×6.354	0.000		
			1×6.321	0.000		
			1×3.352	0.000	1×2.490	
			1×3.354	0.000	1×2.417	
			1×3.341	0.000	1×2.418	
			1×3.339	0.000	1×2.492	
			$1 \times \mathbf{4.527}$	0.848	1×2.394	
			2×6.011	0.000	1×2.577	
			1×5.991	0.000	1×2.578	
			1×5.993	0.000	1×2.396	
O _u –O _u (conf. 3, 2NN)	2.263	2×2.073	1×3.351	0.000	1×2.557	0.000
			1×3.338	0.000	1×2.327	
			1×3.347	0.000	1×2.324	
			1×3.324	0.000	1×2.625	
			1×4.539	0.000	1×2.368	
			1×5.981	0.000	1×2.391	
			1×5.965	0.000		
O _u –O _u (conf. 4, 3NN)	2.205	1×2.077 1×2.078				0.000

Table 2 (continued)

Site	E_{ads} (eV)	$d_{\text{Ag-O}}$ (Å)	$d_{\text{Ag-Ce}}$ (Å)	$\mu_{\text{Ce}}(\mu_{\text{B}})$	$d_{\text{Ce-O}}$ (Å)	$\mu_{\text{Ag}}(\mu_{\text{B}})$
Ce-top (conf. 1)	1.358	2×2.316	1×6.009	0.000	1×2.548	0.000
			1×6.003	0.000		
			1×6.422	0.000		
			1×6.331	0.000		
			1×6.324	0.861		
			1×6.395	0.000		
			1×2.927	0.000	2×2.276	
			2×4.749	0.000	1×2.541	
			2×4.730	2×0.501	1×2.452	
Ce-top (conf. 2, 2NN)	1.670	1×2.293 1×2.326	1×2.944	0.000	1×2.225	0.000
			1×4.912	0.972	1×2.534	
			2×4.774	0.000	2×2.321	
			1×4.599	0.000	1×2.595	
					1×2.387	
					1×2.661	

Distances between Ag and reduced Ce are labelled in bold.

different from the case of the $\text{O}_{\text{u}}-\text{O}_{\text{u}}$ site for $\text{M}/\text{CeO}_2(111)$, in which the 1NN, 2NN and 3NN Ce ions are at the surface. All three considered sites would provide different configurations with the excess electron localized on Ce ions which are different neighbors to the adsorbed atoms. For the convenience of comparison, the delocalized configurations, which are less stable than the localized ones, are also listed in Tables 1–3, although the configuration reported in this work refers to the localized one unless otherwise explicitly stated.

3.1. $\text{Cu}/\text{CeO}_2(100)$

Table 1 summarizes the adsorption energies, E_{ads} (eV), from Eq. (1), relevant bond lengths and magnetic spin moments for all the possible adsorption configurations of Cu adsorbed on $\text{CeO}_2(100)$ surface. $d_{\text{Cu-Ce}}$ is the distance (Å) from adsorbed Cu to 1NN, 2NN or 3NN Ce ion; $d_{\text{Cu-O}}$ is the distance between the adsorbed Cu and the nearest neighboring O ion; $d_{\text{Ce-O}}$ (Å) is the $\text{Ce}^{3+}-\text{O}$ bond length; μ_{Ce} and μ_{Cu} are spin moments (μ_{B}) of Ce and Cu, respectively. Integers that precede $d_{\text{Cu-O}}$ and $d_{\text{Cu-Ce}}$ denote the numbers of NN O and Ce ions relative to the adsorbed Cu atom, respectively. We can clearly see that, among the three types of adsorption sites, the adsorption of Cu atom at the two-fold $\text{O}_{\text{u}}-\text{O}_{\text{u}}$ site exhibits the largest adsorption energies (3.916, 3.920 and 4.079 eV depending on the location of Ce^{3+} relative to the Cu atom). The second stable one is the adsorption at the Ce-top site with two-fold coordinated Cu–O bonds (2.638 eV). The adsorption energies (2.296, 2.316 and 2.376 eV) at the O_{u} site are slightly smaller than that at the Ce-top site. On the other hand, Note that difference between adsorption energies of any two configurations at the O_{u} or $\text{O}_{\text{u}}-\text{O}_{\text{u}}$ site is relatively minor (0.004–0.163 eV) and that a distribution of these configurations could be present in the experiments. Distribution of Ti^{3+} (Ce^{3+}) sites on the reduced $\text{TiO}_2(110)$ ($\text{CeO}_2(111)$) surface is a good example of such a process, in which several Ti^{3+} (Ce^{3+}) sites are close in energy [44,53]. Both the Cu–O bond lengths (1.81–1.91 Å) for $\text{O}_{\text{u}}-\text{O}_{\text{u}}$ and Ce-top sites are close to the experimental value of 1.86 Å [54] in cubic Cu_2O . The Cu–O bond length (1.77 Å) for the O_{u} site is slightly shorter than those for the other two adsorption configurations due to only a single oxygen atom bonded with the Cu.

Based on the configurations proposed above, we calculated isosurfaces of excess spin density for a Cu atom adsorbed on $\text{CeO}_2(100)$. As shown in Fig. 3, the isosurfaces, which are denoted by the black contour lobes in each of Fig. 3(a)–(h), represent the difference between the spin up and spin down moments at given Ce and Cu sites. The localized spin electrons on Ce sites in Fig. 3 have f (f_{xyz}) characteristics [55]. The contour lobes are therefore

indicative of charge transfer from the Cu atom to one of the Ce sites (1NN, 2NN or 3NN) listed in the first column of Table 1 due to the local configuration that results from the applied distortion and relaxation (denoted as conf.). Except for the conf. 1 of Ce-top site where two 2NN Ce^{4+} ions are both partially reduced (see the smallest μ_{Ce} and shortest $d_{\text{Ce-O}}$ values in Table 1), all other adsorption configurations involve the complete reduction of NN Ce^{4+} ions, as indicated by magnetic spin moments among 0.86 and $0.96\mu_{\text{B}}$ which are close to the ideal moment of $1\mu_{\text{B}}$ per Ce^{3+} [56]. Furthermore, the local environments of the Ce ions differ from one another due to the larger size of the Ce^{3+} ion compared with the Ce^{4+} ion. The average distances between surface (or subsurface) Ce^{3+} ions and the neighboring O ions for the respective configurations are in the range of 2.43–2.57 Å, which are larger than the eight-fold theoretical and experimental bond length (2.38 and 2.34 Å) of $\text{Ce}^{4+}-\text{O}$ in cubic CeO_2 (lattice constants of 5.49 and 5.41 Å), but are comparable to the average experimental $\text{Ce}^{3+}-\text{O}$ bond length of 2.455 and 2.542 Å in cubic (space group: Ia-3, six-fold, 206) and hexagonal (space group: P3-M1, seven-fold, 164) Ce_2O_3 [57]. This suggests that the adsorption is accompanied by the reduction of Ce^{4+} to Ce^{3+} .

For the most energetically favorable configuration of Cu at the two-fold $\text{O}_{\text{u}}-\text{O}_{\text{u}}$ site, the transferred charge localized at one 1NN Ce ion leads to a $0.96\mu_{\text{B}}$ spin moment, indicating the reduction of $\text{Ce}^{4+} \rightarrow \text{Ce}^{3+}$. The corresponding spin density isosurface is shown in Fig. 3(d). Fig. 3(e) and (f) shows isosurfaces for the energetically less favorable conf. 2, 2NN (the electron localized on the Ce ion at the subsurface) and conf. 3, 3NN where charge is localized to the f orbitals of the 2NN and 3NN Ce ions relative to the adsorbed Cu. Fig. 3(a)–(c) shows spin density contours at O_{u} sites due to the associated distortions ($d_{\text{Ce-O}}$ (Å)) listed in Table 1 as well as the position of the Cu ion after optimization. From our calculations, the most energetically favorable configuration is Cu adsorption at the two-fold $\text{O}_{\text{u}}-\text{O}_{\text{u}}$ site with the electron localized at the first nearest neighbor (1NN) Ce ion (located at the surface); this has a computed adsorption energy of 4.08 eV. This is quite different from the adsorption behaviors of Cu on $\text{CeO}_2(111)$ and $\text{CeO}_2(110)$, in which the adsorptions at the three-fold O_{d} site with the excess electron localized at the third nearest neighbor (3NN) Ce ion and at the two-fold $\text{O}_{\text{u}}-\text{O}_{\text{u}}$ site with the electron localized at the second nearest neighbor (2NN) Ce ion are the most energetically favorable [15,17]. On the other hand, for the same adsorption model, the adsorption of a Cu atom on $\text{CeO}_2(100)$ is more energetically favorable than those on $\text{CeO}_2(111)$ and $\text{CeO}_2(110)$ [15,17], suggesting that the more reactive sites exist on $\text{CeO}_2(100)$ compared with those on $\text{CeO}_2(111)$ and $\text{CeO}_2(110)$. Fig. 3(g) shows spin density contours for a Cu atom adsorbed at Ce-top site (conf. 1) in which the excess electron is

Table 3

Adsorption energies, bond lengths and magnetic spin moments of metal atoms for the adsorption configurations of Au atom on CeO₂(100). For a given adsorption site, configuration numbers (e.g. conf. 2, 1NN) are associated with the distortion applied to Ce–O distances listed as $d_{\text{Ce–O}}$, which are the bond lengths between the Ce³⁺ and the nearest neighboring O ions. The undistorted $d_{\text{Ce–O}}$ is 2.38 Å. E_{ads} is the computed adsorption energy, $d_{\text{Au–O}}$ is the distance between the adsorbed Au and the nearest O ions (an O ion for the O_u site and two O ions for the O_u–O_u and Ce-top sites), and $d_{\text{Au–Ce}}$ are distances from the adsorbed Au to 1NN, 2NN, and 3NN Ce ions (1NN, the first nearest neighbor, 2NN, the second nearest neighbor and 3NN, the third nearest neighbor Ce ion from the Au adatom), respectively, following geometry optimization. Note that integers in $d_{\text{Au–O}}$ (Å) and $d_{\text{Au–Ce}}$ (Å) denote the number of O and Ce ions, respectively, within the distances relative to the adsorbed Au ion. Magnetic spin moments of reduced Ce (in bold) and oxidized Au ions are, respectively, μ_{Ce} and μ_{Au} .

Site	E_{ads} (eV)	$d_{\text{Au–O}}$ (Å)	$d_{\text{Au–Ce}}$ (Å)	$\mu_{\text{Ce}}(\mu_{\text{B}})$	$d_{\text{Ce–O}}$ (Å)	$\mu_{\text{Au}}(\mu_{\text{B}})$
O _u (conf. 1)	1.234	1 × 1.970	1 × 3.800	0.496	1 × 2.408	0.000
			1 × 3.800	0.495	2 × 2.270	
			4 × 5.375	0.000	1 × 2.592	
			2 × 6.210	0.000	1 × 2.219	
O _u (conf. 2, 1NN)	1.458	1 × 1.970	2 × 6.679	0.000	1 × 2.422	0.000
			1 × 3.749	0.000	1 × 2.319	
			1 × 3.879	0.956	1 × 2.326	
			1 × 5.315	0.000	1 × 2.337	
			1 × 5.330	0.000	1 × 2.458	
			1 × 5.447	0.000	1 × 2.519	
			1 × 5.461	0.000	1 × 2.711	
			1 × 6.231	0.000		
			1 × 6.236	0.000		
			1 × 6.488	0.000		
			1 × 6.888	0.000		
			1 × 3.803	0.000	1 × 2.336	
O _u (conf. 3, 2NN)	1.355	1 × 1.973	1 × 3.810	0.000	1 × 2.340	0.000
			1 × 5.276	0.000	1 × 2.410	
			1 × 5.305	0.000	1 × 2.418	
			1 × 5.327	0.951	1 × 2.599	
			1 × 5.329	0.000	1 × 2.600	
			1 × 6.162	0.000		
			1 × 6.172	0.000		
			1 × 6.627	0.000		
			1 × 6.655	0.000		
			1 × 3.795	0.000	1 × 2.332	
O _u (conf. 4, 3NN)	1.361	1 × 1.974	1 × 3.810	0.000	1 × 2.337	0.000
			1 × 5.365	0.000	1 × 2.385	
			1 × 5.366	0.000	1 × 2.426	
			2 × 5.373	0.000	1 × 2.545	
			1 × 6.609	0.000	1 × 2.609	
			2 × 6.228	0.000		
			1 × 6.642	0.949		
			4 × 3.208	4 × 0.277	1 × 2.443	
			1 × 4.266	0.000	1 × 2.248	
O _u –O _u (conf. 1)	2.655	2 × 2.027	2 × 5.762	0.000	1 × 2.274	0.000
			2 × 5.801	0.000	1 × 2.542	
			4 × 6.317	0.000	1 × 2.189	
					1 × 2.405	
					1 × 2.327	
O _u –O _u (conf. 2, 1NN)	3.039	1 × 2.021	1 × 3.180	0.000	1 × 2.327	0.000
		1 × 2.027	1 × 3.184	0.000	1 × 2.346	
			1 × 3.248	0.000	1 × 2.351	
			1 × 3.261	0.962	1 × 2.487	
			1 × 4.276	0.000	1 × 2.603	
			1 × 5.766	0.000	1 × 2.661	
			1 × 5.768	0.000		
			1 × 5.782	0.000		
			1 × 5.850	0.000		
			1 × 6.261	0.000		
			1 × 6.297	0.000		
			1 × 6.333	0.000		
			1 × 6.943	0.000		
			1 × 3.216	0.000	1 × 2.399	
O _u –O _u (conf. 3, 2NN)	2.846	1 × 2.023	1 × 3.220	0.000	1 × 2.420	0.000
		1 × 2.024	2 × 3.230	0.000	1 × 2.426	
			1 × 4.283	0.853	1 × 2.486	
			1 × 5.796	0.000	1 × 2.487	
			1 × 5.800	0.000	1 × 2.581	
			1 × 5.826	0.000	1 × 2.572	
			1 × 5.827	0.000	1 × 2.396	
			1 × 6.326	0.000		
			1 × 6.328	0.000		
			1 × 6.333	0.000		
			1 × 3.193	0.000	1 × 2.334	
O _u –O _u (conf. 4, 3NN)	2.966	2 × 2.025	1 × 3.208	0.000	1 × 2.347	0.000
			1 × 3.217	0.000	1 × 2.388	
			1 × 3.221	0.000	1 × 2.416	
			1 × 4.280	0.000		

Table 3 (continued)

Site	E_{ads} (eV)	$d_{\text{Au-O}}$ (Å)	$d_{\text{Au-Ce}}$ (Å)	$\mu_{\text{Ce}}(\mu_{\text{B}})$	$d_{\text{Ce-O}}$ (Å)	$\mu_{\text{Au}}(\mu_{\text{B}})$
Ce-top (conf. 1)	0.944	2×2.252	1×5.760	0.000	1×2.558	0.000
			1×5.791	0.000	1×2.622	
			1×5.800	0.000		
			1×5.820	0.000		
			1×6.261	0.940		
			1×6.331	0.000		
			1×6.352	0.000		
			1×6.955	0.000		
			1×2.795	0.000	1×2.211	
			2×4.667	0.000	2×2.281	
			2×4.669	2×0.523	1×2.433	
					1×2.514	
Ce-top (conf. 2, 2NN)	1.052	1×2.192 1×2.306	1×2.807	0.000	1×2.314	0.000
			1×4.581	0.000	1×2.315	
			1×4.673	0.000	1×2.358	
			1×4.671	0.000	1×2.543	
			1×4.762	0.929	1×2.592	
					1×2.622	

Distances between Au and reduced Ce are labelled in bold.

delocalized at the 2 s nearest neighboring (2NN) Ce ions and the adsorption energy of 2.221 eV is the lowest among all the considered adsorption configurations. Interestingly, if some structural distortions are made, the conf. 1 at the Ce-top site will evolve into the conf. 2 (see Fig. 3(h)), in which the excess electron is localized on one 2NN Ce^{4+} ion and the adsorption energy increases to 2.638 eV.

For all configurations associated with each adsorption site, the interaction between the Cu atom and $\text{CeO}_2(100)$ surface involves a charge transfer from the adsorbate to the substrate, yielding the oxidization of Cu atom and the reduction of a Ce ion. Here we take the most energetically favorable adsorption configuration (conf. 1, 1NN of $\text{O}_{\text{u}}-\text{O}_{\text{u}}$ site) for an example and analyze the respective partial density of states (PDOS) of Cu atom, pure $\text{CeO}_2(100)$ and Cu/ $\text{CeO}_2(100)$ as shown in Fig. 4(a)–(c), respectively. In Fig. 4(a), there are occupied spin-up and unoccupied spin-down states just below and above the E_{F} which correspond to the Cu-4s state; occupied spin-up and spin-down states are the Cu-3d state. For pure $\text{CeO}_2(100)$, the highest occupied valence band in Fig. 4(b) results from O-2p and some contribution from the Ce-4f, suggesting Ce-4f/O-2p hybridization [46] (herein O atom refers to the one which bonds with Cu atom and Ce atom refers to the one which is reduced upon the Cu adsorption.). We can clearly see that, compared to the PDOS of the isolated Cu atom in Fig. 4(a), the adsorption of Cu atom at an $\text{O}_{\text{u}}-\text{O}_{\text{u}}$ site (conf. 2 1NN) on $\text{CeO}_2(100)$ causes the occurrence of a new state just below E_{F} and the disappearance of Cu-4s state (see Fig. 4(c)). This indicates that the single Cu-4s¹ electron has been transferred. Simultaneously, there is a new occupied peak corresponding to the Ce-4f states for the Cu/ $\text{CeO}_2(100)$ system. By comparing the PDOS among the same adsorption configurations of Cu adsorbed on $\text{CeO}_2(100)$, (110) and (111), it is found that the Cu/ $\text{CeO}_2(100)$ exhibits the strongest Cu-3d/O-2p orbital hybridization interaction, followed by Cu/ $\text{CeO}_2(110)$ and Cu/ $\text{CeO}_2(111)$. This is also consistent with the relationship among the adsorption energies of Cu on three surfaces. Moreover, the Cu-4s¹ electron localizes on the 1NN Ce ion, resulting in reduction of the Ce^{4+} ion to Ce^{3+} and oxidation of the Cu atom to Cu^+ . This observation is supported by the experimental result [58], which indicates that Cu^+ species are always catalytic centers with CeO_2 playing a support role.

3.2. Ag/ $\text{CeO}_2(100)$

Following the same methodology, we consider the same adsorption sites and adsorption configurations as in the case of Cu.

Table 2 summarizes the adsorption energies, the location of Ce^{3+} , the Ag–O, Ag–Ce and Ce–O bond lengths, and magnetic spin moments of Ag and Ce. It is found that the adsorption at the two-fold $\text{O}_{\text{u}}-\text{O}_{\text{u}}$ site with the excess electron localized at the first nearest neighbor (1NN) Ce ion (conf. 2, 1NN) is the most energetically favorable, followed by those at the Ce-top and O_{u} sites. The stability sequence for the Ag adsorption at the various sites on $\text{CeO}_2(100)$ surface is similar to that for the Cu adsorption. For three adsorption configurations of Ag at the $\text{O}_{\text{u}}-\text{O}_{\text{u}}$ site, the computed E_{ads} is lower by 1.642 (conf. 2, 1NN), 1.653 (conf. 3, 2NN) and 1.715 (conf. 4, 3NN) eV than those of Cu, whereas the respective adsorptions of Ag at the Ce-top and O_{u} sites are less stable by 0.968 and 0.755–0.939 eV than those of Cu. This is consistent with relationship between the Ag–O and Cu–O bond lengths for the same adsorption model. Among all three considered sites, the Ag–O bond lengths are 2.062–2.326 Å whereas the Cu–O bond lengths are 1.768–1.907 Å. Note that for the adsorption at the $\text{O}_{\text{u}}-\text{O}_{\text{u}}$ or O_{u} site, the Ag–O distances of 2.062–2.078 Å are in close accordance with the experimental value of 2.05 Å in cubic Ag_2O [59].

In the similar situation to Cu, the adsorption of Ag atom at different sites has different configurations. For the O_{u} or $\text{O}_{\text{u}}-\text{O}_{\text{u}}$ site, there are three adsorption configurations in which the $\text{Ag}^+-\text{Ce}^{3+}$ distances are different (see the fourth column in Table 2). They are separated by the adsorption energy differences of 0.058–0.232 eV and correspond to the locations of Ce^{3+} at the 1NN, 2NN and 3NN relative to the Ag, respectively, in which the 1NN and 3NN are in the surface (the second atomic layer) whereas the 2NN is in the subsurface (the fourth atomic layer). For the Ce-top site, the slight structural distortion based on the conf. 1, in which the excess electron is delocalized at the 2 s nearest neighboring (2NN) Ce ions, results in the increase of the adsorption energy by 0.312 eV and the complete localization of the excess electron at a single 2NN Ce ion.

According to Table 2, we can see that upon the adsorption of Ag on $\text{CeO}_2(100)$, there is always one electron transferred for all the configurations. In most cases, the transferred electron localizes at one Ce^{4+} ion, making it reduced to Ce^{3+} , accompanying the oxidation of Ag atom into Ag^+ ion. Fig. 5 compares the PDOS of a Ag atom (Fig. 5(a)), pure $\text{CeO}_2(100)$ (Fig. 5(b)) and the most energetically favorable $\text{O}_{\text{u}}-\text{O}_{\text{u}}$ configuration (conf. 2, 1NN) for Ag/ $\text{CeO}_2(100)$ (Fig. 5(c)). As is the case for a Cu adatom, there is a new occupied peak corresponding to the Ce-4f state; the occupied Ag-5s state completely disappears (Fig. 5(c)). This implies that the Ag adatom is oxidized to Ag^+ , whereas the corresponding Ce^{4+} is reduced to Ce^{3+} . This is consistent with calculated results of Ag adsorbed on

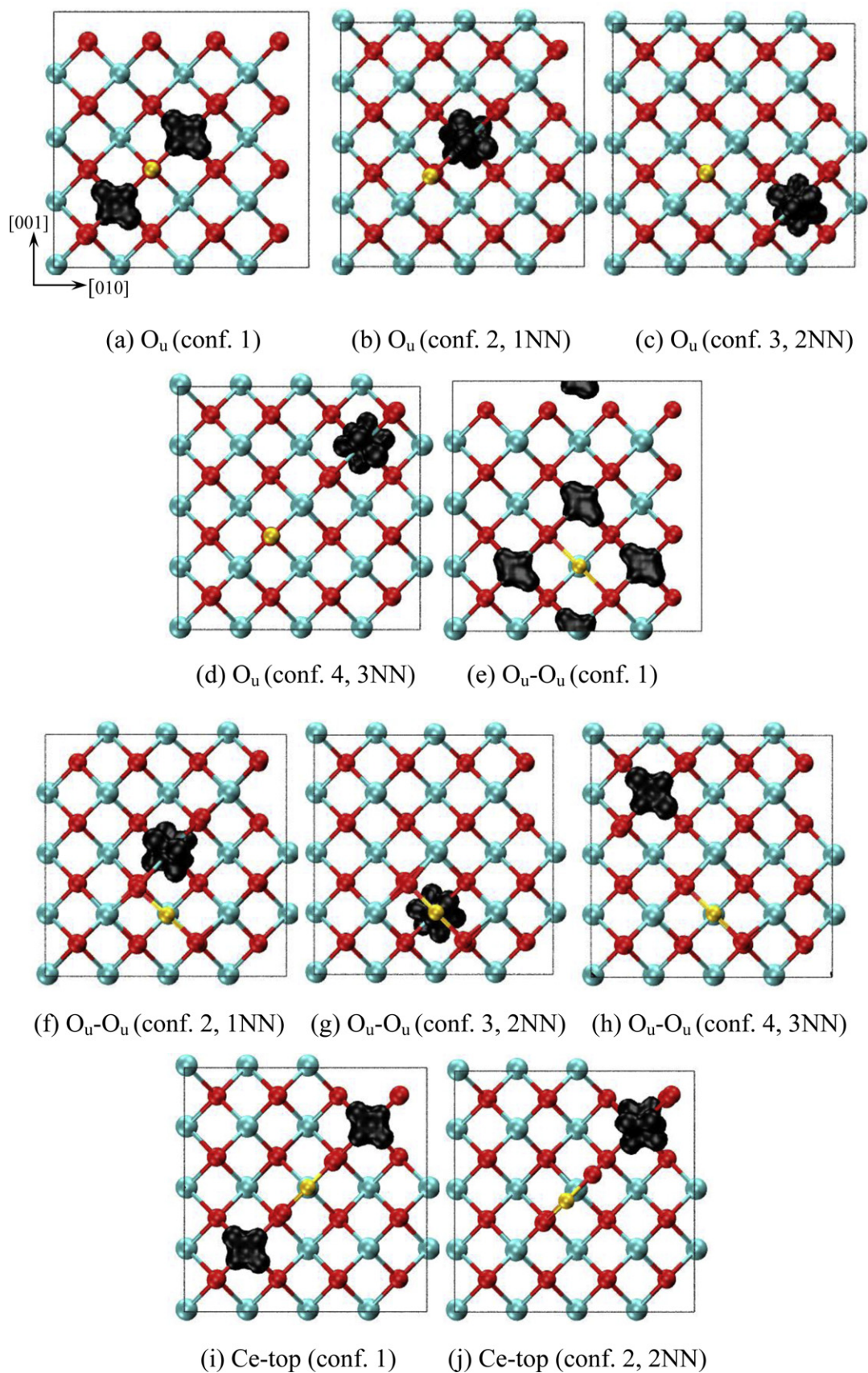


Fig. 3. Isosurfaces of excess spin density for Cu adsorbed (a) O_u (conf. 1), (b) O_u (conf. 2, 1NN), (c) O_u (conf. 3, 2NN), (d) O_u (conf. 4, 3NN), (e) O_u-O_u (conf. 1), (f) O_u-O_u (conf. 2, 1NN), (g) O_u-O_u (conf. 3, 2NN), (h) O_u-O_u (conf. 4, 3NN), (i) Ce-top (conf. 1), (j) Ce-top (conf. 2, 2NN) on $CeO_2(100)$. Isosurfaces correspond to the location of Ce^{3+} ions after initial structural distortions followed by geometry optimization. Values of isosurfaces are $0.002e \text{ \AA}^{-3}$ in (a)–(j).

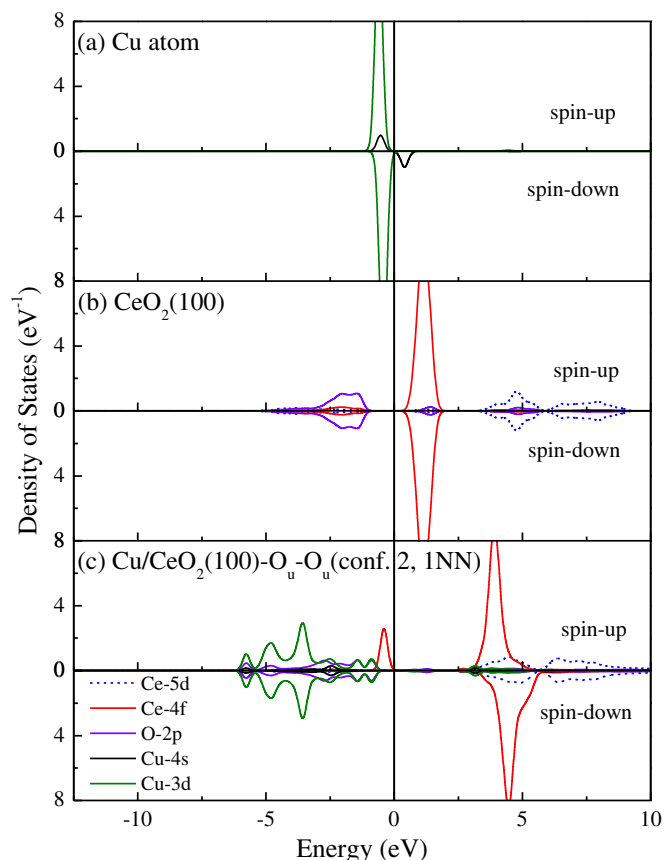


Fig. 4. Partial density of states (PDOS) of (a) Cu atom, (b) pure $\text{CeO}_2(100)$ and (c) Cu adsorbed on $\text{O}_u\text{--O}_u$ site (conf. 2, 1NN). Zero energy corresponds to the Fermi energy, E_F . Upper and lower panels represent spin up and spin down, respectively.

$\text{CeO}_2(111)$ and (110) surfaces, in which the adsorbed Ag is oxidized to Ag^+ [15,17]. Experimentally, X-ray photoelectron spectroscopy (XPS) analysis of Sarode et al. [60] indicates that the high catalytic activity of Ag in Ag/CeO_2 is attributed to the presence of Ag^+ species dispersed on CeO_2 surface.

3.3. $\text{Au}/\text{CeO}_2(100)$

Au/CeO_2 catalyst exhibits good catalytic activities in several important oxidation reactions [9,61–63] and $\text{Au}/\text{CeO}_2(111)$ and $\text{Au}/\text{CeO}_2(110)$ have been extensively investigated [16,64–66]. However, far less is known about $\text{Au}/\text{CeO}_2(100)$. Table 3 summarizes the adsorption energies, the location of Ce^{3+} , the relevant Au–O, Au–Ce and Ce–O bond lengths, and magnetic spin moments of Ag and Ce for all the adsorption configurations. Similar to the cases of Cu and Ag, the adsorption configuration at the two-fold $\text{O}_u\text{--O}_u$ site, in which one 1NN Ce^{4+} relative to the Au atom is reduced to Ce^{3+} with a magnetic moment of $0.96\mu_B$ and the Au atom is oxidized to Au^+ , is the energetically most favorable ($E_{\text{ads}} = 3.039$ eV). Different from those of Cu and Ag at the Ce-top site, the second stable configuration of Au on $\text{CeO}_2(100)$ is at the O_u site.

Similar to the cases of Cu and Ag, there are different configurations of Au on $\text{CeO}_2(100)$ with the excess electron located at various neighboring Ce ion and they are separated by the adsorption energy differences of 0.006–0.193 eV (see the fourth column in Table 3). Note that the conf. 3, 2NN and conf. 4, 3NN at the O_u site have the same adsorption energies (1.355 vs. 1.361 eV). For the configuration at the Ce-top site, as compared with the delocalized solution, an 0.108 eV increase of the adsorption energy for Au,

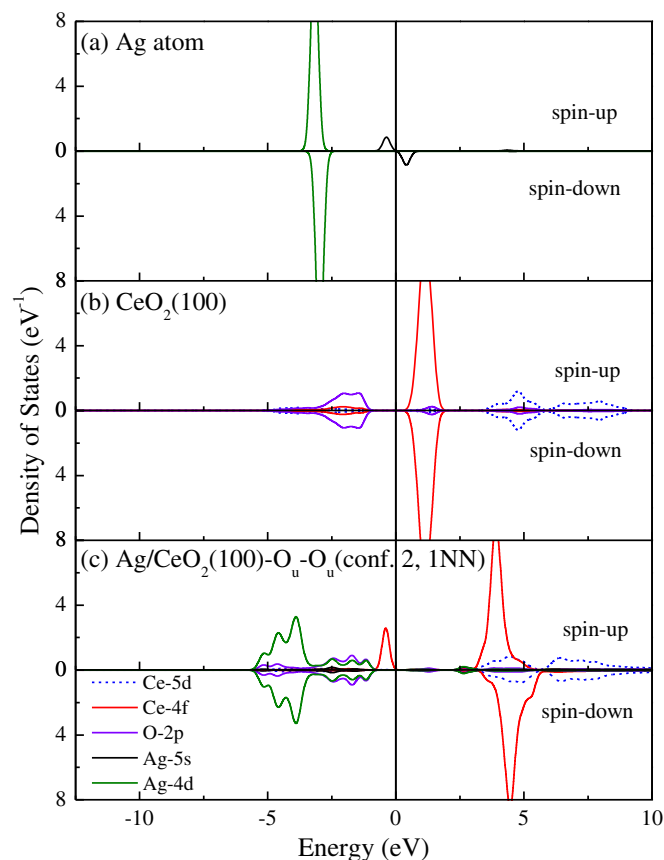


Fig. 5. Partial density of states (PDOS) of (a) Ag atom, (b) pure $\text{CeO}_2(100)$ and (c) Ag adsorbed on $\text{O}_u\text{--O}_u$ site (conf. 2, 1NN). Zero energy corresponds to the Fermi energy, E_F . Upper and lower panels represent spin up and spin down, respectively.

which is derived from the slight structural distortion and the resultant complete localization of excess electron, is smaller than 0.417 eV for Cu and 0.312 eV for Ag.

Fig. 6 shows the PDOS of an isolated Au atom (Fig. 6(a)), pure $\text{CeO}_2(100)$ (Fig. 6(b)) and the most energetically favorable $\text{O}_u\text{--O}_u$ (conf. 2, 1NN) configuration (Fig. 6(c)) for $\text{Au}/\text{CeO}_2(100)$. Fig. 6(c) shows that the adsorption of Au atom causes the occurrence of a new occupied peak corresponding to localized Ce-4f states. The occupied Au-6s state in Fig. 6(a) disappears in Fig. 6(c), indicating that Au indeed loses an electron. Experimental and theoretical studies [67–70] proved that Au^+ could be considered as an active site for the adsorption of CO in the WGS reactions. Also, experiment [71] carried out by Qian et al. revealed that the existence of Au^+ in the Au/CeO_2 system has promoted the formation of surface vacancies which play a key role in the redox reaction.

3.4. Discussion

For all three considered adsorption sites on $\text{CeO}_2(100)$, Cu, Ag and Au atoms exhibit the similar adsorption characteristics. The adsorption at the two-fold $\text{O}_u\text{--O}_u$ site is the most energetically favorable. At the $\text{O}_u\text{--O}_u$ or O_u site, there are three different configurations with the excess electron (from the M atom) at various neighboring Ce ions (denoted as 1NN, 2NN and 3NN). Their stability sequence follows $E_{\text{ads}}(1\text{NN}) > E_{\text{ads}}(3\text{NN}) > E_{\text{ads}}(2\text{NN})$ for Cu and Au. However, the case of Ag is an exception, in which the stability sequence is $E_{\text{ads}}(3\text{NN}) > E_{\text{ads}}(1\text{NN}) > E_{\text{ads}}(2\text{NN})$ at the O_u site and $E_{\text{ads}}(1\text{NN}) > E_{\text{ads}}(2\text{NN}) > E_{\text{ads}}(3\text{NN})$ at the $\text{O}_u\text{--O}_u$ site. Interestingly, the conf. 3, 2NN and conf. 4, 3NN at the $\text{O}_u\text{--O}_u$ site have almost the

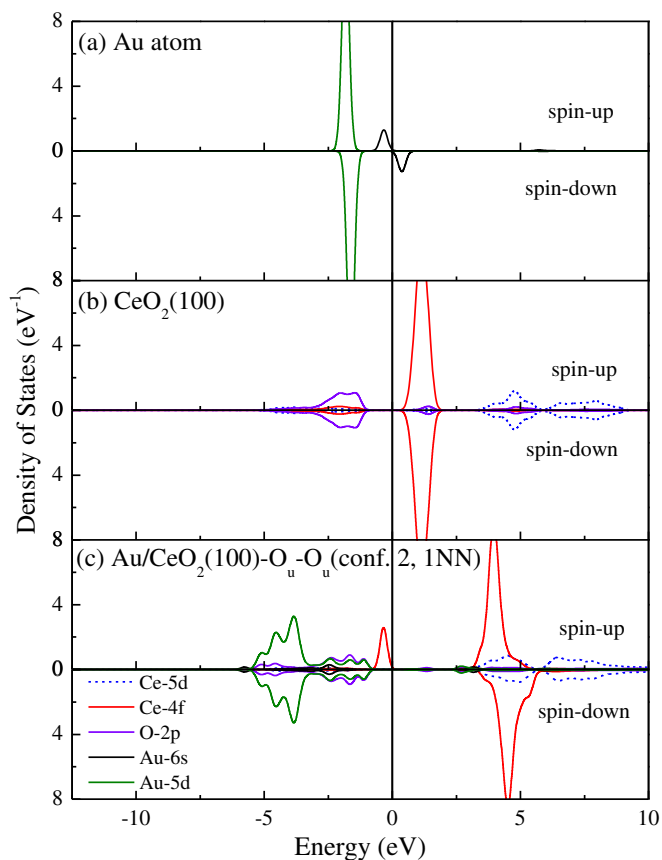


Fig. 6. Partial density of states (PDOS) of (a) Au atom, (b) pure $\text{CeO}_2(100)$ and (c) Au adsorbed on $\text{O}_u\text{--O}_u$ site (conf. 2, 1NN). Zero energy corresponds to the Fermi energy, E_F . Upper and lower panels represent spin up and spin down, respectively.

same adsorption energies although the 2NN and 3NN Ce ions are located in the subsurface and surface, respectively. For the Ce-top site, there are two configurations in which the excess electron is delocalized at the two 2NN Ce ions and localized at a single 2NN Ce ion, respectively, and the latter has the higher adsorption energy than the former.

There are some differences among the adsorption behaviors of M ($M = \text{Cu}, \text{Ag}, \text{Au}$) on $\text{CeO}_2(111)$, $\text{CeO}_2(110)$ and $\text{CeO}_2(100)$ that require clarification. For each given site on $\text{CeO}_2(111)$ and $\text{CeO}_2(110)$, the adsorption configuration with the excess electron located at the surface Ce ion away from the M atom is energetically favorable. The opposite, however, is true for the M atom adsorption on $\text{CeO}_2(100)$ with the exception of the adsorption of Ag atom at the O_u site. In addition, it is worth mentioning that the adsorption of Cu atom on $\text{CeO}_2(110)$ can result in Cu^{2+} [17], an oxidation state that is not predicted by DFT calculations of Cu adsorption on $\text{CeO}_2(111)$ and $\text{CeO}_2(100)$. The orders on the adsorption energy of M ($M = \text{Cu}, \text{Ag}, \text{Au}$) on a given low-index surface follow $\text{Cu} > \text{Au} > \text{Ag}$ for $\text{CeO}_2(100)$ and $\text{CeO}_2(110)$ and $\text{Cu} > \text{Ag} > \text{Au}$ for $\text{CeO}_2(111)$. On the other hand, $M/\text{CeO}_2(100)$ ($M = \text{Cu}, \text{Ag}, \text{Au}$) system exhibits the largest adsorption energy, followed by $M/\text{CeO}_2(110)$ and $M/\text{CeO}_2(111)$, which is consistent with the relationship among the surface energies of $\text{CeO}_2(100)$, (110) and (111) surfaces. The most reactive surface, (100), [22–32,72] provides more reactive sites than the (111) and (110) surfaces for interaction with M ($M = \text{Cu}, \text{Ag}, \text{Au}$). There are compelling experimental results that support this conclusion [33,34].

The importance of investigating single metal atom on CeO_2 surface arises from a number of reasons, including (i) nanocluster

growth proceeds by the anchoring of one atom on CeO_2 surface, which determines future growth pathways of the nanoclusters, and (ii) the interaction of the metal atom with CeO_2 surface can be probed by a number of experimental techniques to investigate the fundamental aspects of the electronic structure of interface between metal atom and CeO_2 surface. It must be emphasized that the localization of the excess electron, both the resultant increase of the adsorption energy and the occurrence of multiple adsorption configurations with the excess electron localized at different neighboring Ce ion are attributed to the effects of the slight structural distortions. For example, for the undistorted configurations of Cu, Ag and Au adsorbed at the Ce-top site, the excess electron is delocalized at two 2NN Ce ions and configurations are not stable with the smaller energies of 0.108–0.417 eV compared with the distorted cases. Similar conclusion has been reached in our previous studies of M adsorption behavior on $\text{CeO}_2(111)$ [15] and (110) [17]. Also, in recent studies of charge transfer behavior caused by the removal an O atom in bulk CeO_2 [42,73] and on $\text{CeO}_2(111)$ [44,45], $\text{CeO}_2(110)$ [74] and $\text{TiO}_2(110)$ [53], it was found that there exist multiple configurations with two excess electrons localized at different Ce^{3+} ions. As mentioned in previous sections, Ce–O distances in each configuration detailed in Tables 1–3 were slightly adjusted to lower the symmetry of the corresponding $M/\text{CeO}_2(100)$ configuration prior to geometry optimization. This provided the local environment that was conducive to the reduction of Ce^{4+} to Ce^{3+} following optimization. Experimentally, these slight structural distortions can result from the introduction of impurities or by manipulation of the crystal morphology during catalytic material preparation [51,52]. The combinations of experimental result with our first-principles modeling deepen the understanding of the catalytic properties of CeO_2 surface supported metal clusters and could also be expanded to other important metal/oxide systems.

4. Conclusions

Adsorption mechanisms of M ($M = \text{Cu}, \text{Ag}, \text{and Au}$) atom on $\text{CeO}_2(100)$ surface have been investigated using the first-principles density functional theory calculations considering the on-site Coulomb interaction within the PBE + U scheme. The systematical analysis of the adsorptions energies, atomic and electronic structures reveals that the order on the adsorption energy follows the sequence of $\text{Cu} > \text{Au} > \text{Ag}$. There are multiple adsorption configurations at a given site, in which the configuration with the excess electron localized at the first nearest neighboring Ce ion to the M is the most energetically favorable. The adsorption behavior of M on $\text{CeO}_2(100)$ is compared with those on $\text{CeO}_2(111)$ and $\text{CeO}_2(110)$.

Acknowledgments

The present work is supported by National 973 Program of China (2012CB215400), National Natural Science Key Foundation of China (NSFC) (No. 50730004), National Natural Science Foundation of China (NSFC) (Nos. 51072183 and 50802089) and Natural Science Foundation of Zhejiang Province (Nos. Y4090280 and Y4100191).

References

- [1] G.A. Deluga, J.R. Salge, L.D. Schmidt, X.E. Verykios, *Science* 303 (2004) 993.
- [2] S.D. Park, J.M. Vohs, R.J. Gorte, *Nature (London)* 404 (2000) 265.
- [3] A. Trovarelli, *Catal. Rev. Sci. Eng.* 38 (1996) 439.
- [4] H. Son, M. Shamsuzzoha, A.M. Lane, *J. Catal.* 210 (2002) 460.
- [5] J.F. Chen, Y.Y. Zhan, J.J. Zhu, C.Q. Chen, X.Y. Lin, Q. Zheng, *Appl. Catal. A: Gen.* 377 (2010) 121.
- [6] J.A. Rodriguez, P. Liu, M. Pérez, G. Liu, J. Hrbek, *J. Phys. Chem. A* 114 (2010) 3802.
- [7] B.R. Kydd, W.Y. Teoh, K. Wong, Y. Wang, J. Scott, Q.-H. Zeng, A.-B. Yu, J. Zou, R. Amal, *Adv. Funct. Mater.* 19 (2009) 369.

- [8] Z.X. Yang, B.L. He, Z.S. Lu, K. Hermansson, *J. Phys. Chem. C* 114 (2010) 4486.
- [9] V. Shapovalov, H. Metiu, *J. Catal.* 245 (2007) 205.
- [10] M.F. Camellone, S. Fabris, *J. Am. Chem. Soc.* 131 (2009) 10473.
- [11] O. Pozdnyakova-Tellinger, D. Teschner, J. Kröhnert, F.C. Jentoft, A. Knop-Gericke, R. Schlögl, A. Wootsch, *J. Phys. Chem. C* 111 (2007) 5426.
- [12] H.-L. Chen, S.-H. Liu, J.-J. Ho, *J. Phys. Chem. B* 110 (2006) 14816.
- [13] G. Avgouropoulos, T. Ioannides, *Catal. Lett.* 116 (2007) 15.
- [14] M.M. Branda, N.C. Hernández, J.F. Sanz, F. Illas, *J. Phys. Chem. C* 114 (2010) 1934.
- [15] Y.H. Tang, H. Zhang, L.X. Cui, C.Y. Ouyang, S.Q. Shi, W.H. Tang, H. Li, L.Q. Chen, *J. Power Sources* 197 (2012) 28.
- [16] N.C. Hernández, R. Grau-Crespo, N.H. de Leeuw, J.F. Sanz, *Phys. Chem. Chem. Phys.* 11 (2009) 5246.
- [17] L.X. Cui, Y.H. Tang, H. Zhang, L.G. Hector Jr., C.Y. Ouyang, S.Q. Shi, H. Li, L.Q. Chen, *Phys. Chem. Chem. Phys.* 14 (2012) 1923.
- [18] N.J. Castellani, M.M. Branda, K.M. Neyman, F. Illas, *J. Phys. Chem. C* 113 (2009) 4948.
- [19] C.J. Zhang, A. Michaelides, D.A. King, S.J. Jenkins, *J. Phys. Chem.* 129 (2008) 194708.
- [20] M.M. Branda, N.J. Castellani, R. Grau-Crespo, N.H. de Leeuw, N.C. Hernandez, J.F. Sanz, K.M. Neyman, F. Illas, *J. Chem. Phys.* 131 (2009) 094702.
- [21] T.X.T. Sayle, S.C. Parker, C.R.A. Catlow, *Surf. Sci.* 316 (1994) 329.
- [22] D.C. Sayle, S.A. Maicaneanu, G.W. Watson, *J. Am. Chem. Soc.* 124 (2002) 11429.
- [23] S.Q. Shi, Y.H. Tang, C.Y. Ouyang, L.X. Cui, X.G. Xin, P.J. Li, W.W. Zhou, H. Zhang, M.S. Lei, L.Q. Chen, *J. Phys. Chem. Solids* 71 (2010) 788.
- [24] Y. Jiang, J.B. Adams, M. van Schilfhaarde, *J. Chem. Phys.* B 123 (2005) 064701.
- [25] M. Baudin, M. Wójcik, K. Hermansson, *Surf. Sci.* 468 (2000) 51.
- [26] J. Stubenrauch, E. Broscha, J.M. Vohs, *Catal. Today* 28 (1996) 431.
- [27] T.X.T. Sayle, S.C. Parker, D.C. Sayle, *Chem. Commun.* 21 (2004) 2438.
- [28] J.P.Y. Tan, H.R. Tan, C. Boothroyd, Y.L. Foo, C.B. He, M. Lin, *J. Phys. Chem. C* 115 (2011) 3544.
- [29] H.R. Tan, J.P.Y. Tan, C. Boothroyd, T.W. Hansen, Y.L. Foo, M. Lin, *J. Phys. Chem. C* 116 (2012) 242.
- [30] Z.L. Wang, X.D. Feng, *J. Phys. Chem. B* 107 (2003) 13563.
- [31] H. Nörenberg, J.H. Harding, *Surf. Sci.* 477 (2001) 17.
- [32] N.V. Skorodumova, M. Baudin, K. Hermansson, *Phys. Rev. B* 69 (2004) 075401.
- [33] K.B. Zhou, X. Wang, X.M. Sun, Q. Peng, Y.D. Li, *J. Catal.* 229 (2005) 206.
- [34] E. Aneggi, J. Llorca, M. Maoro, A. Trovarelli, *J. Catal.* 234 (2005) 88.
- [35] V. Trtik, F. Sánchez, R. Aguiar, Y. Maniette, C. Ferrater, M. Varela, *Appl. Phys. A* 67 (1998) 455.
- [36] P.E. Blöchl, *Phys. Rev. B* 50 (1994) 17953.
- [37] G. Kresse, J. Furthmüller, *Phys. Rev. B* 54 (1996) 11169.
- [38] J.P. Perdew, K. Burke, M. Ernzerhof, *Phys. Rev. Lett.* 77 (1996) 3865.
- [39] S.L. Dudarev, G.A. Botton, S.Y. Savrasov, C.J. Humphreys, A.P. Sutton, *Phys. Rev. B* 57 (1998) 1505.
- [40] S. Fabris, S. de Gironcoli, S. Baroni, G. Vicario, G. Balducci, *Phys. Rev. B* 72 (2005) 237102.
- [41] M. Cococcioni, S. de Gironcoli, *Phys. Rev. B* 71 (2005) 035105.
- [42] Y.H. Tang, H. Zhang, L.X. Cui, C.Y. Ouyang, S.Q. Shi, W.H. Tang, H. Li, J.S. Lee, L.Q. Chen, *Phys. Rev. B* 82 (2010) 125104.
- [43] J.L.F. Da Silva, M.V. Ganduglia-Pirovano, J. Sauer, V. Bayer, G. Kresse, *Phys. Rev. B* 75 (2007) 045121.
- [44] M.V. Ganduglia-Pirovano, J.L.F. Da Silva, J. Sauer, *Phys. Rev. Lett.* 102 (2009) 026101.
- [45] H.-Y. Li, H.-F. Wang, X.-Q. Gong, Y.-L. Guo, Y. Guo, G.Z. Lu, P. Hu, *Phys. Rev. B* 79 (2009) 193401.
- [46] S.Q. Shi, X.Z. Ke, C.Y. Ouyang, H. Zhang, H.C. Ding, Y.H. Tang, W.W. Zhou, P.J. Li, M.S. Lei, W.H. Tang, *J. Power Sources* 194 (2009) 830.
- [47] S.J. Duclos, Y.K. Vohra, A.L. Ruoff, A. Jayaraman, G.P. Espinosa, *Phys. Rev. B* 38 (1988) 7755.
- [48] L. Gerward, J.S. Olsen, *Powder Diff.* 8 (1993) 127.
- [49] H.J. Monkhorst, J.D. Pack, *Phys. Rev. B* 13 (1976) 5188.
- [50] P.E. Blöchl, O. Jepsen, O.K. Andersen, *Phys. Rev. B* 49 (1994) 16223.
- [51] X. Wang, J.C. Hanson, G. Liu, J.A. Rodriguez, A. Iglesias-Juez, M. Fernandez-Garcia, *J. Chem. Phys.* 121 (2004) 5434.
- [52] P. Krüger, S. Bourgeois, B. Domenichini, H. Magnan, D. Chandesris, P. Le Fèvre, A.M. Flank, J. Jupille, L. Floreano, A. Cossaro, A. Verdini, A. Morgante, *Phys. Rev. Lett.* 100 (2008) 055501.
- [53] N.A. Deskins, R. Rousseau, M. Dupuis, *J. Phys. Chem. C* 115 (2011) 7562.
- [54] A. Kirfel, K.D. Eichhorn, *Acta Cryst. A* 46 (1990) 271.
- [55] X. Han, J. Lee, H.-I. Yoo, *Phys. Rev. B* 79 (2009) 100403.
- [56] N.V. Skorodumova, R. Ahuja, S.I. Simak, I.A. Abrikosov, B. Johansson, B.I. Lundqvist, *Phys. Rev. B* 64 (2001) 115108.
- [57] N. Hirosaki, S. Ogata, C. Kocer, *J. Alloys Compd.* 351 (2003) 31.
- [58] A. Hornés, A.B. Hungria, P. Bera, A.L. Cámara, M. Fernández-García, A. Martínez-Arias, L. Barrio, M. Estrella, G. Zhou, J.J. Fonseca, J.C. Hanson, J.A. Rodriguez, *J. Am. Chem. Soc.* 132 (2010) 34.
- [59] T. Suzuki, *J. Phys. Soc.* 15 (1960) 2018.
- [60] P.R. Sarode, K.R. Priolkar, P. Bera, M.S. Hegde, S. Emura, R. Kumashiro, *Mater. Res. Bull.* 37 (2002) 1679.
- [61] P.Y. Sheng, G.A. Bowmaker, H. Idriss, *Appl. Catal. A: Gen.* 261 (2004) 171.
- [62] F. Arena, P. Famulari, G. Trunfio, G. Bonura, F. Frusteri, L. Spadaro, *Appl. Catal. B: Environ.* 66 (2006) 81.
- [63] F. Romero-Sarria, A. Penkova, L.M. Martinez, M.A. Centeno, K. Hadjiivanov, J.A. Odriozola, *Appl. Catal. B: Environ.* 84 (2008) 119.
- [64] F. Ying, S. Wang, C.-T. Au, S.-Y. Lai, *Microporous Mesoporous Mater.* 142 (2011) 308.
- [65] A. Karpenko, R. Leppelt, V. Plzak, R.J. Behma, *J. Catal.* 252 (2007) 231.
- [66] D. Widmann, R. Leppelt, R.J. Behm, *J. Catal.* 251 (2007) 437.
- [67] J.G. Wang, B. Hammer, *Phys. Rev. Lett.* 97 (2006) 136107.
- [68] S. Minicò, S. Scirè, C. Crisafulli, A.M. Visco, S. Galvagno, *Catal. Lett.* 47 (1997) 273.
- [69] T.M. Salama, T. Shido, H. Minagawa, M. Ichikawa, *J. Catal.* 152 (1995) 322.
- [70] P. Bera, M.S. Hegde, *Catal. Lett.* 79 (2002) 75.
- [71] K. Qian, S.S. Lv, X.Y. Xiao, H.X. Sun, J.Q. Lu, M.F. Luo, W.X. Huang, *J. Mol. Catal. A: Chem.* 306 (2009) 40.
- [72] T.X.T. Sayle, S.C. Parker, D.C. Sayle, *Phys. Chem. Chem. Phys.* 7 (2005) 2936.
- [73] E. Shoko, M.F. Smith, R.H. McKenzie, *J. Phys. Condens. Matter* 22 (2010) 223201.
- [74] M. Nolan, *Chem. Phys. Lett.* 499 (2010) 126.